1998 Nature America Inc. • http://structbio.nature.com

Solution structure of a protein inhibitor of neuronal nitric oxide synthase

The structure of the neuronal nitric oxide synthase inhibitory protein, PIN (protein inhibitor of nNOS), has been determined by NMR spectroscopy. Two N-terminal antiparallel α-helices pack against a four-stranded antiparallel β-sheet in the C-terminal region of the protein, forming a two-layer α/β plait. The three dimensional structure of PIN resembles the fold of the B-chain of aspartylglucosaminidase. A non-prolyl *cis* peptide bond was found between Pro 52 and Thr 53 of the protein. PIN has a large solvent-exposed hydrophobic surface that contains a cavity and is rimmed with positive charges. This surface may serve as the primary target-binding region for this multi-functional regulatory protein.

Neuron-derived nitric oxide (NO) plays numerous roles in neuronal cell functions. In the peripheral nervous system, NO acts as a nonadrenergic-noncholinergic neurotransmitter mediating the actions of autonomic motor neurons on smooth muscle[1,2]. NO has also been implicated to play important roles in synaptic plasticity in the central nervous system. Nitric oxide synthase (NOS) inhibitors block hippocampal long-term potentiation, a model of learning and memory[1,3]. In addition to its physiological roles as a signaling molecule in the peripheral and central nervous systems, NO is neurotoxic at abnormally high concentrations. Over-activity of N-methyl-D-aspartic (NMDA) receptors has been implicated in numerous neurodegenerative diseases including stroke, Alzheimer's disease, and Huntington's disease[1,4,5]. The essential physiological roles, as well as the potential toxicity, of NO in neuronal cells require the tight regulation of NO biosynthesis. In the brain, NO is produced predominantly by the neuronal isoform of NOS (nNOS)[6]. The influx of calcium following the activation of NMDA receptors allows Ca^{2+}-calmodulin to bind to and then activate nNOS. Apart from the regulation of NO levels by self-degradation in the cellular environment, the synthesis of NO is also subject to direct inhibition. One example is the inhibition of nNOS by a recently identified protein inhibitor called PIN (protein inhibitor of nNOS)[7]. The protein was found to bind to nNOS and destabilize the dimeric structure of the enzyme, thereby inhibiting the enzyme activity[7].

PIN is highly conserved throughout the evolution (Fig. 1) and is ubiquitously expressed in different cell types[8,9]. The protein has also been implicated in many functions other than regulating nNOS activity[7,8,10,11]. The extremely high amino acid sequence conservation and broad cellular functions suggest that PIN is likely to be a multifaceted regulatory protein, analogous to the ubiquitous Ca^{2+}-signalling protein calmodulin. Here, we have determined the three dimensional structure of PIN using NMR spectroscopy. The functional significance of the PIN structure is discussed.

Description of the structure

The three-dimensional structure of PIN was solved using a total of 2,009 experimental restraints derived from multidimensional heteronuclear NMR spectroscopy (Table 1). Fig. 2*a* shows a stereoview of the best-fit superposition of the family of 20 final structures of PIN. As a result of the large number of experimental restraints (22.6

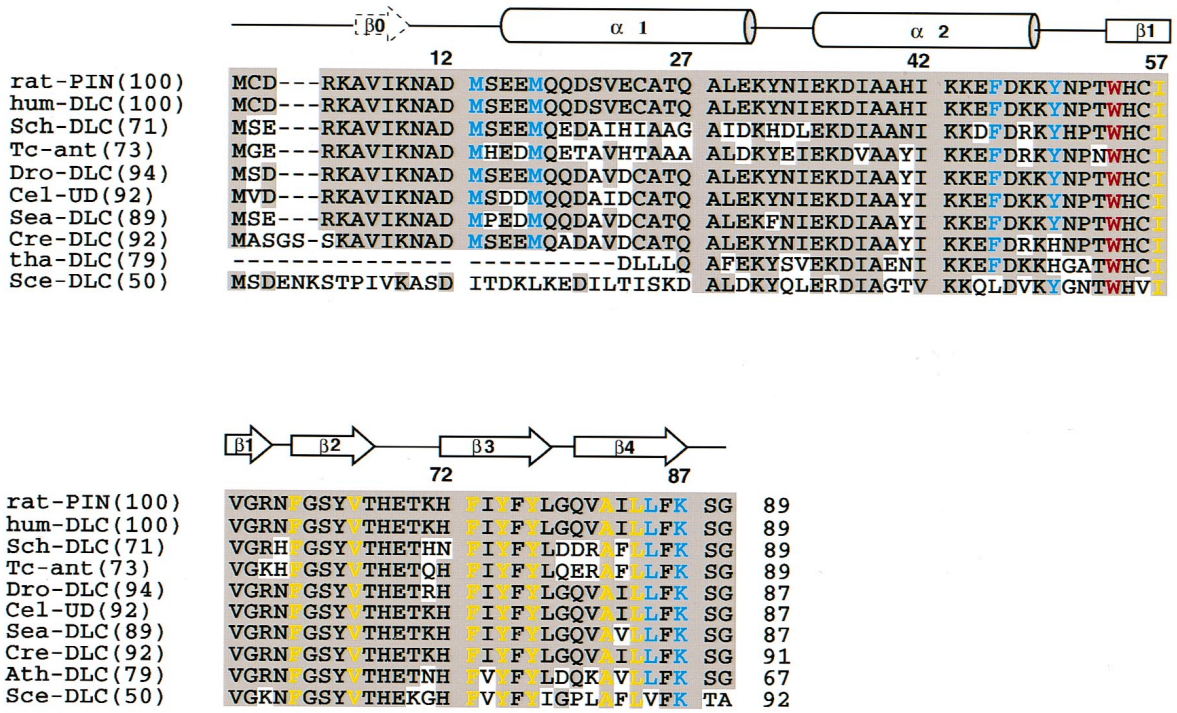

Fig. 1 Sequence alignment of PIN and its homologs from various species. The secondary structure of PIN, determined in this work, is indicated above the sequence of PIN. The color/shaded regions represent the identical amino acids among the sequences. The percentage sequence identity to PIN is also included in parenthesis following each sequence name. The amino acid residues located in the solvent-exposed surface area are highlighted in yellow. Trp 54 is color-coded in red, and the hydrophobic amino acid residues surrounding Trp 54 are colored in blue (see Fig. 3*d*). The sequences and their abbreviated name and genebank accession code are: PIN from rat (rat–PIN), human dynein light chain (DLC, hum-DLC, U32944), *Schistosoma mansoni* DLC (Sch-DLC, U55992), *Schistosoma mansoni* T-cell-stimulating antigen (Tc-ant, X98619), *Drosophila melanogaster* DLC (Dro-DLC, U32855), *Caenorhabditis elegans* DLC (Cel-DLC, U00043), Sea Urchin DLC (Sea-DLC, AB004830), *Chlamydomonas reinhardtii* DLC (Cre-DLC, A56444), *Arabidopsis thaliana DLC* (tha-DLC, Z97340), and *Saccharomyces cerevisiae* DLC (Sce-DLC, S66142).

1998 Nature America Inc. • http://structbio.nature.com

letters

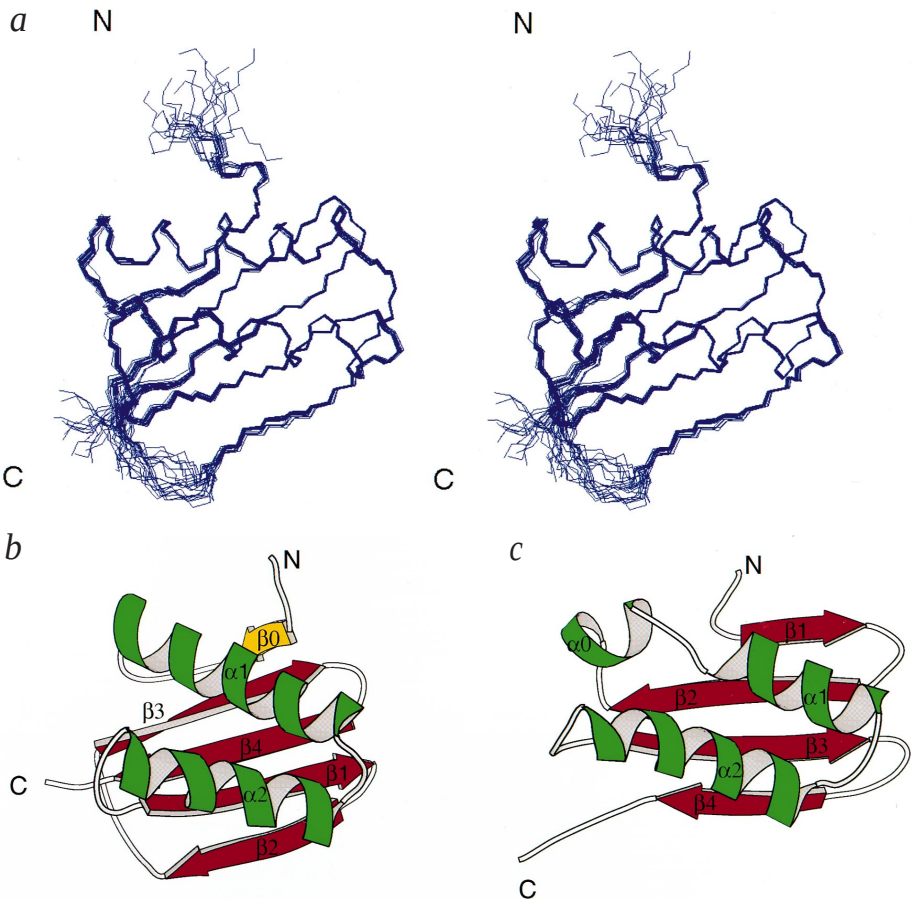

Fig. 2 ***a***, Stereo view showing the best-fit superposition of the backbone atoms (N, Cα, and C') of the final 20 structures of PIN. The structures are superimposed against the energy-minimized average structure using the residues with well-defined structures (residues 5–67 and 72–87). The N- and C-termini of the protein are indicated (panel prepared using INSIGHT II, Biosym, San Diego, California.). Comparison of the topology of ***b***, PIN and ***c***, the B-chain of aspartylglucosaminidase (AGA). The numbering of the helices and strands in AGA is arbitrary, and follows that of PIN. The folding unit of B-chain of AGA comprises amino acid residues from B218 to B298 (panel prepared using MOLSCRIPT[29]).

restraints per residue), we have been able to determine the structure of the protein to a high resolution. The overall backbone precision (root-mean-square (r.m.s.) deviation) of the structural ensembles shown in Fig. 2*a* is 0.27 Å for the secondary structural regions (residues 5–67 and 72–87), and 0.43 Å for amino acid residues from 5–87. The structural statistics are summarized in Table 1.

Other than the first three residues at the N-terminus, the last two residues at the C-terminus, and the four residues (His 68–Lys 71) connecting β2 and β3, PIN adopts a well-defined structure in solution. The protein is a mixed α-helix/β-sheet protein. It contains two long helices: α1 (residues 15–31) and α2 (35–49); and four β-strands: β1 (54–60), β2 (62–67), β3 (72–78), and β4 (81–87). The two α-helices are essentially antiparallel to each other, and the four β-strands form a flat antiparallel sheet (Fig. 2*b*). NOE analysis of the backbone NH and αH protons of amino acid residues from Ala 6–Lys 9 and those of Tyr 75–Leu 78 in β3 showed that these two peptide segments may form an antiparallel β-sheet-like structure[12]. However, inspection of the final calculated structures indicated that the dihedral angles of the amino acid residues from Ala 6–Lys 9 deviate slightly from the standard β-strand structure, suggesting the formation of an irregular β-strand structure.

Chemical shift index[13] analysis also revealed a break in the β-strand structure of this region at Ile 8. Therefore, we term the fragment from Ala 6–Lys 9 as β0 to indicate the irregularity of the strand. Both α-helices of the protein make direct contacts with the β-sheet, and are located at the center of one side of the β-sheet to form a two-layer α/β plait (Fig. 2*b*). The loop that connects β2 and β3 is poorly defined, and likely to undergo conformational averaging under the NMR conditions, as we observed extensive peak broadening for the backbone and side chain resonances of these residues.

Similarity to aspartylglucosaminidase

To find out whether the two-layer α/β plait seen in PIN represents a novel fold, we searched the Protein Data Bank (PDB) using the program Dali[14]. A database search revealed that a folding unit in the B-chain of aspartylglucosaminidase (AGA; PDB code 1apy)[15] is closely related to the fold of PIN (Fig. 2*c*). The fold from the B-chain of AGA contains four β-strands, and these four β-strands form an antiparallel β-sheet that closely resembles the β-sheet of PIN. However, due to topological differences, the β-strand pairing orders between the two proteins are different (Fig. 2*b*,*c*). The B-chain of AGA also contains two α-helices (α1 and α2) that are similar to those of PIN. The α1 helix of AGA is shorter than the α1 helix of PIN and corresponds to the C-terminal part of α1 of PIN. However, a short α-helix (α0) is found at the N-terminus of AGA α1. The combined length of the α0 and α1 helices is roughly equal to the length of α1 of PIN (Fig. 2*b*,*c*). Superposition of the backbones of two molecules using the corresponding secondary structural units (the four β-strands and two α-helices) give rise to an r.m.s. deviation of 2.4 Å. It is possible that the two-layer α/β fold observed in PIN represents a novel member of the growing protein fold family.

Non-prolyl *cis*-peptide bond

PIN contains two restrained linkers that allow abrupt changes in the main chain directions. β-strands 1 and 2 are connected by a very tight turn (Arg 60 and Phe 62) with only one residue (Asn 61) not involved in the hydrogen-bonding network of the β-sheet. Helix 2 and strand 1 are also linked with a restrained four-residue loop (Tyr 50-Asn 51-Pro 52-Thr 53) which allows a sudden direction change of the main chain. The four-residue α2/β1 linker is

1998 Nature America Inc. • http://structbio.nature.com

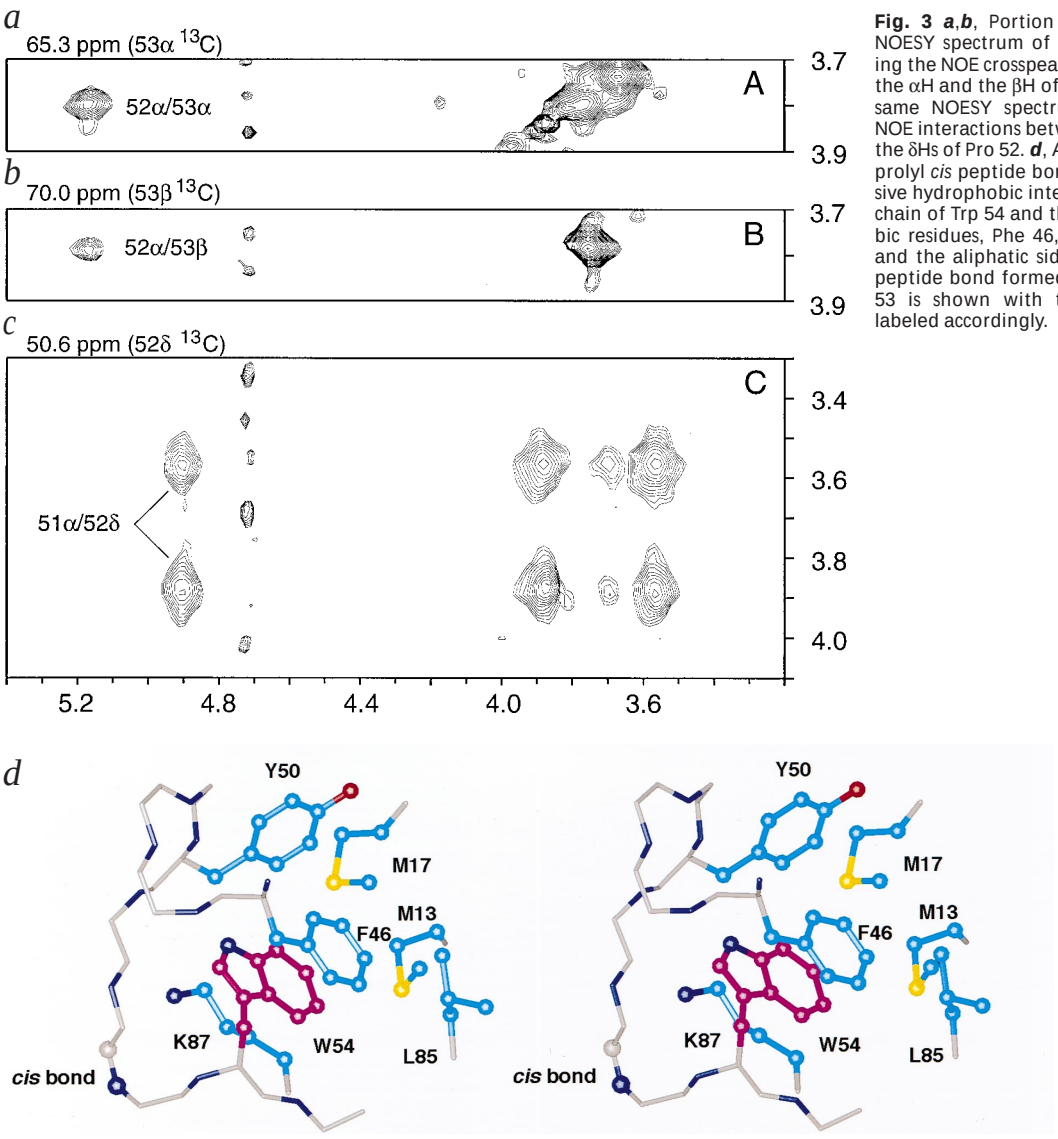

Fig. 3 ***a***,***b***, Portion of the ^{13}C-separated 3D NOESY spectrum of ^{15}N,^{13}C-labelled PIN showing the NOE crosspeaks of the αH of Pro 52 with the αH and the βH of Thr 53 respectively. ***c***, The same NOESY spectrum showing the intense NOE interactions between the αH of Asn 51 and the δHs of Pro 52. ***d***, A close-up view of the non-prolyl *cis* peptide bond of PIN. Note the extensive hydrophobic interactions between the side chain of Trp 54 and the surrounding hydrophobic residues, Phe 46, Met 13, Met 17, Leu 85, and the aliphatic side chain of Lys 87. The *cis* peptide bond formed between Pro 52 and Thr 53 is shown with the ball-stick model and labeled accordingly.

particularly worth noting. A strong NOE between the αH of Pro 52 and the αH of Thr 53 was observed in the NOESY spectrum of the protein (Fig. 3*a*). This strong, sequential αH NOE clearly shows the existence of a *cis*-peptide bond between Pro 52 and Thr 53 of the protein. The NOEs between the αH of Pro 52 and the side chain protons of Thr 53 further support the existence of the *cis*-peptide bond (Fig. 3*b*). It should be noted that this non-prolyl *cis* peptide bond exists immediately next to the Pro 52, and this proline residue adopts a *trans* peptide bond as indicated by the strong NOEs between αH of Asn 51 and the two δHs of Pro 52 (Fig. 3*c*). It is unusual that a proline residue (Pro 52) should adopt a *trans* bond, while the peptide bond of the following residue (Thr 53) adopts an energetically unfavorable *cis* bond. The occurrence of *cis* peptides bond is rare (0.3% of all peptide bonds), with the non-prolyl *cis* peptide bonds even rarer (about 0.03% of all peptide bonds)[16,17]. In the cases where non-prolyl *cis* peptide bonds have been studied, almost all play significant roles in catalysis or have other functional roles[17,18]. It will, therefore, be interesting to uncover the possible functional role of the non-prolyl *cis* peptide bond of PIN.

Both experimental and theoretical studies have shown that a *cis* peptide bond can destabilize a folded protein by 15–20 kJ mol^{-1} (ref. 16 and refs therein). However, we have shown that PIN is a highly stable protein in solution, with a melting point of ~63 °C (M.Z., unpublished). Therefore, the energy penalty created by the *cis* peptide bond must be compensated by favorable interactions both locally and globally in order to maintain the stability of the protein. Careful examination of the PIN structure provides a possible structural basis that may explain the stability of this unusual *cis* peptide bond. NOE analysis and amide exchange data showed that neither the side chain nor the backbone of Thr 53 are involved in the interactions to stabilize the *cis* peptide bond (data not shown). Rather, we observed extensive hydrophobic interactions between the side chain of Trp 54 and the side chains of a number of other amino acids (Fig. 3*d*). In particular, the indole ring of Trp 54 and the benzene ring of Phe 46 are very closely packed though a π-stacking interaction (the distance between the centers of the two rings is 3.3 Å). The close proximity, and the parallel orientation of the two aromatic rings is nearly energetically optimal, and such π-stacking interactions make large energy contributions to stabilize the *cis* peptide bond through van der Waals contacts in proteins[19]. In addition to the π-stacking interaction, the other face of the Trp 54 indole ring is 'sandwiched' with the aliphatic side chain of Lys 87. Furthermore, the base of the Trp indole ring is surrounded by the side chains of Met 13, Met 17, and Leu 85 (Fig. 3*d*). These side

1998 Nature America Inc. • http://structbio.nature.com

letters

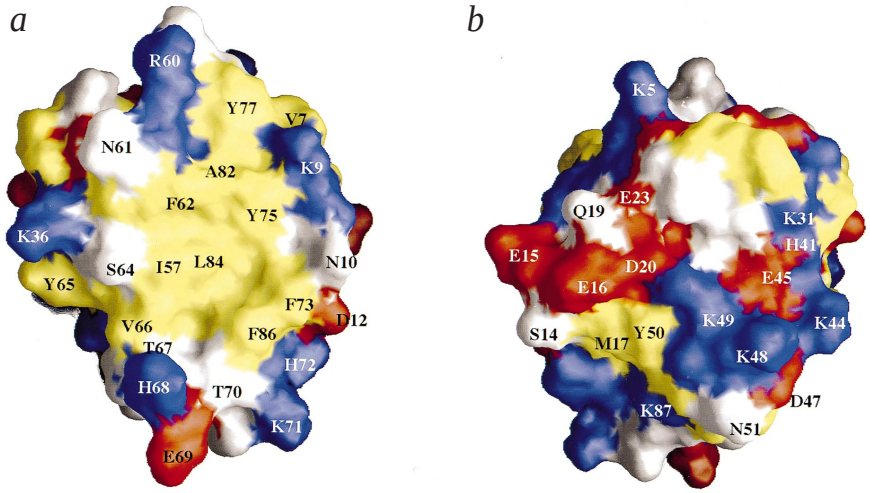

Fig. 4 Molecular surface representation of PIN showing ***a***, the solvent-exposed hydrophobic surface area and ***b***, the hydrophilic surface, rotated by 180° with respect to the view in (*a*). The hydrophobic residues (Ala, Ile, Leu, Met, Pro, Phe, Trp, Try, and Val) are shown in yellow, negatively charged residues (Asp and Glu) in red, positively charged residues (Arg, His, and Lys) in magenta, and polar residues (Asn, Cys, Gln, Gly, Ser, and Thr) in gray. The figure was prepared using GRASP[30].

chains, together with side chains of Phe 46 and Lys 87, form a hydrophobic 'trap' enclosing the side chain of Trp 54, thereby forcing the Pro 52–Thr 53 peptide bond to adopt a *cis* conformation (Fig. 3*d*).

Functional implications

The PIN-binding domain of nNOS was mapped to a 17-residue peptide fragment using NMR and biochemical approaches (Fan *et al*., submitted). Database searches found no sequences that were homologous to this peptide. Given that PIN interacts with multiple protein targets[7,8,10,11], this implies that the PIN-binding domains of its various targets probably share no amino acid sequence homology. To elucidate the possible mechanism of the interactions between PIN and its targets, we analyzed the molecular surface properties of the protein.

Fig. 4*a* shows the surface of the solvent-exposed side of the β-sheet of the protein, revealing that PIN contains a long and relatively wide hydrophobic strip that is solvent-exposed. The hydrophobic surface is surrounded by a number of positively charged amino acid residues. We also detect a deep cavity at the bottom of the hydrophobic surface strip (Fig. 4*a*). The existence of a large solvent-exposed hydrophobic patch containing a cavity is reminiscent of the surface of Ca^{2+}-calmodulin[20]. It is interesting to note that calmodulin binds to over 30 target peptides with different amino acid sequences[21]. In addition, the hydrophobic surface of calmodulin is also surrounded by a number of charged residues, although these residues have opposite charges to those of PIN. Therefore, calmodulin-binding peptides generally contain positively charged residues[21]. In contrast, inspection of the amino acid sequence of the PIN-binding domain of nNOS (one letter code sequence: M^{228}KDTGIQVDRDLDGKSH^{244}; Fan *et al*., submitted) shows that the center of this 17-residue peptide contains three negatively charged Asp residues. It is possible that the negatively charged Asp residues of the nNOS peptide form salt bridges with the positively charged residues located at the rim of the hydrophobic surface of PIN. The PIN-binding peptide of nNOS also contains a number of hydrophobic residues in the middle of its sequence (underlined). PIN may be able to bind to multiple targets with different amino acid sequences using its solvent-exposed hydrophobic surface, and positively charged rim, in a mode similar to that of calmodulin binding to its target peptides[21].

Chemical shift perturbation studies show that the amino acid residues in the hydrophobic surface of PIN undergo large chemical shift changes upon binding to the PIN-binding domain of nNOS, suggesting that the solvent exposed hydrophobic surface is indeed involved in the binding of nNOS (Fan *et al*., submitted). In the absence of PIN-binding peptides, PIN can undergo self-aggregation at high concentrations (Fan *et al*., submitted). The concentration dependent aggregation of PIN is most likely to be non-specific as no inter-molecular NOEs could be observed using a mix ^{13}C,^{15}N-labeled and unlabeled PIN sample (data not shown). In addition, sedimentation equilibrium studies also showed that the association between PIN molecules is weak (Fan *et al*., submitted). It is possible that this concentration-dependent self-aggregation is mediated through the solvent-exposed surface area of the protein. Such weak, non-specific aggregation is unlikely to bear significant biological relevance.

Fig. 4*b* shows the surface representation of PIN (rotated by 180° with respect to Fig. 4*a*). It can be seen that this side of the PIN surface is predominantly hydrophilic. In particular, it contains a high concentration of charged amino acid residues. The distribution of the charges is not even on the surface with one end being more positively charged and the other more negatively charged (Fig. 4*b*). This specific localization of the charges suggests that it may be possible that this side of the PIN is also involved in protein–protein interaction. PIN may be able to bind to different targets using two very different surfaces. The existence of two possible target-binding surfaces with entirely different properties may partially explain the lack of sequence similarity between the PIN-binding domains of its different targets. A detailed explanation of the interaction mechanisms between PIN and its targets awaits the determination of the three-dimensional structures of the complexes of PIN and its binding peptides.

Methods

Sample preparation. Rat PIN was cloned into the pET-14b vector (Novagene), and expressed in and purified from *Escherichia coli* BL21(DE3) cells as described elsewhere (Fan *et al*., submitted). All NMR samples were dissolved in 100 mM potassium phosphate buffer, pH 6.0 containing 2 mM d_{10}-DTT. The concentration of NMR samples was ~1.5 mM.

NMR spectroscopy: All NMR experiments were performed at 30 °C on a four-channel Varian Inova 500 MHz spectrometer equipped with an actively *z*-gradient shielded triple-resonance probe. Sequential backbone resonance assignments were achieved by through-bond heteronuclear correlation experiments including HNCACB, CBCA(CO)NH, HNCO and (HB)CBCACO(CA)HA, and the non-aromatic side-chain assignments were obtained using an HCCH-TOCSY experiment[22]. The aromatic rings were assigned using homonuclear 2D ^1H-NOESY spectra[12]. Stereo-specific assignment of the methyl groups of Val and Leu residues were obtained using a fractionally ^{13}C-labeled PIN

1998 Nature America Inc. • http://structbio.nature.com

sample[23]. The backbone coupling constants, $^3J_{NH\alpha}$, were estimated from a ^1H-^{15}N HMQC-J experiment[24] recorded on a ^{15}N-labeled sample in H_2O. All NMR data were processed with the NMRPipe[25], and analyzed with PIPP and STAPP[26].

Structural calculation. Approximate interproton distances were obtained from a 3D ^{15}N-separated (mixing time 100 ms), a ^{13}C-separated (mixing time 100 ms), and homonuclear ^1H 2D (mixing times 50 and 100 ms) NOESY spectra. The distance restraints were grouped into three classes for NOEs unrelated to NH protons, 1.8–2.7, 1.8–3.3, and 1.8–5.0 Å, corresponding to strong, medium and weak NOEs. The NOEs involving backbone NH protons were grouped into four distance ranges, 1.8–2.9, 1.8–3.5, 1.8–5.0, and 1.8–5.9 Å, corresponding to strong, medium, weak, and very weak NOEs. Phi and psi dihedral angle restraints were derived from the $^3J_{NH\alpha}$ coupling constants and chemical shift indices[13]. Values of -60° ± 30° and -40° ± 30° were used for phi and psi dihedral angles respectively, for α-helical regions and -120 ± 50° and 120 ± 50° for β-strands. Hydrogen bond restraints were obtained by analyzing the $^1H/^2H$ exchange rates and standard backbone NOE patterns characteristic of α-helices or β-strands. Two distance restraints, $r_{NH\text{-}O}$ (1.8–2.2 Å) and $r_{N\text{-}O}$ (2.2–3.3 Å), were used for each hydrogen bond. Structures were calculated using a standard distance geometry/simulated annealing protocol[27] using the program X-PLOR 3.1[28].

Coordinates. The coordinates of the structures together with the restraints have been deposited in the Brookhaven Protein Data Bank (accession codes 1bkq and r1bkqmr).

Table 1 Structural statistics for the family of 20 PIN structures[1]

Distance restraints	
Intraresidue (i-j = 0)	597
Sequential (|i-j| = 1)	424
Medium-range (2 ≤ |i-j| ≤4)	336
Long-range (|i-j| ≥ 5)	473
Hydrogen bonds	80
Total	1910
Dihedral–angle restraints	
Φ	50
Ψ	49
Total	99
Mean r.m.s. deviations from the experimental restraints	
Distance (Å)	0.023 ± 0.001
Dihedral-angle (°)	0.36 ± 0.03
Mean r.m.s. deviations from idealized covalent geometry	
Bonds (Å)	0.004 ± 0.000
Angles (°)	0.61 ± 0.01
Impropers (°)	0.52 ± 0.02
Mean energies (kcal mol^{-1})	
E_{NOE}[2]	51.2 ± 3.2
E_{cdih}[2]	0.77 ± 0.14
E_{repel}	113.0 ± 3.2
$E_{L\text{-}J}$	-316.0 ± 9.3
Ramachandran plot[3]	
% residues in the most favorable region	
Residues 5–87	75.3
Secondary structures	84.9
Atomic r.m.s. differences (Å)[4]	
Residues 5–87	
Backbone atoms	0.43 ± 0.06
Heavy atoms	0.99 ± 0.08
Residues 5–67, 72–87	
Backbone atoms	0.27 ± 0.05
Heavy atoms	0.76 ± 0.05

[1]None of the structures exhibits distance violations greater than 0.2 Å or dihedral angle violations greater than 3°.
[2]The final values of the square-well NOE and dihedral-angle potentials were calculated with force constants of 50 kcal mol^{-1} Å^{-2} and 200 kcal mol^{-1} rad^{-2} respectively.
[3]The program PROCHECK[31] was used to assess the overall quality of the structures.
[4]The precision of the atomic coordinates is defined as the average r.m.s. difference between the 20 final PIN structures and the mean coordinates of the protein. The backbone atoms comprise the N, Cα, C' and O atoms.

Acknowledgments
We thank L.E. Kay for providing NMR pulse sequences, M. Nilges for the advice in the structure calculation, and D. Smith for careful reading and critical comments of the manuscript. This work is partially supported by an RGC grant to M.Z. from the Research Grant Committee of Hong Kong. The NMR spectrometer used in this work was purchased by the Biotechnology Research Institute, the Hong Kong University of Science and Technology.

Hidehito Tochio, Shinya Ohki, Qiang Zhang, Ming Li and Mingjie Zhang

Department of Biochemistry, The Hong Kong University of Science and Technology, Clear Water Bay, Kowloon, Hong Kong, P. R. China.

Correspondence should be addressed to M.Z. *email: mzhang@uxmail.ust.hk*

Received 17 July, 1998; accepted 11 September, 1998.

1. Brenman, J.E., & Bredt, D.S. *Meth. Enz.*. **269**, 119–129 (1996).
2. Rand, M.J., & Li, C.G. *Ann. Rev. Physiol.* **57**, 659–682 (1995).
3. Garthwaite, J. & Boulton, C.L. *Ann. Rev. Physiol.* **57**, 683–706 (1995).
4. Lipton, S.A., & Rosenberg, P.A. *N. England J. Med.* **330**, 613–22 (1994).
5. Choi, D.W. *Prog. Brain Res.* **100**, 47–51 (1994).
6. Huang, P.L., Dawson, T.M., Bredt, D.S., Snyder, S.H., & Fishman, M.C. *Cell* **75**, 1273–1286 (1993).
7. Jaffrey, S.R., & Snyder, S.H. *Science* **274**, 774–777 (1996).
8. Dick, T., Ray, K., Salz, H.K., & Chia, W. *Mol. Cell. Biol.* **16**, 1966–1977 (1996).
9. Greenwood, M.T., Guo, Y., Kumar, U., Beauséjours, S., & Hussain, S.N.A. *Biochem. Biophys. Res. Commun.* **238**, 617–621 (1997).
10. King, S.M., & Patel-King, R. S. *J. Biol. Chem.* **270**, 11445–11452 (1995).
11. King, S.M. *et al. J. Biol. Chem.* **271**, 19358–19366 (1996).
12. Wüthrich, K. *NMR of Proteins and Nucleic Acids.* (Wiley, New York; 1986).
13. Wishart, D.S., & Sykes, B.D. *Meth. Enz.*. **239**, 363–392 (1994).
14. Holm, L. & Sander, C. *J. Mol. Biol.* **233**, 123–38 (1993).
15. Oinonen, C., Tikkanen, R., Rouvinen, J., & Peltonen, L. *Nature Struct. Biol.* **2**, 1102–1108 (1995).
16. Stewart, D.E., Sarkar, A., & Wampler, J.E. *J. Mol. Biol.* **214**, 253–260 (1990).
17. Weiss, M.S., Jabs, H, & Hilgenfeld, R. *Nature Struct. Biol.* **5**,–676 (1998).
18. Herzberg, O., & Moult, J. *Proteins: Struct. Funct. Genet.* **11**, 223–229 (1991).
19. McGaughey, G.B., Gagné, M., & Rappé, A.K. *J. Biol. Chem.* **273**, 15458–15463 (1998).
20. Babu, Y.S., Bugg, C.E., & Cook, W.J. *J. Mol. Biol.* **204**, 191–204 (1988).
21. Zhang, M. & Yuan, T. *Biochem. Cell Biol.* **in the press**.
22. Bax, A., & Grzesiek, S. *Acc. Chem. Res.* **26**, 131–138 (1993).
23. Neri, D., Szyperski, T. Otting, G., Senn, H., & Wüthrich, K. *Biochemistry* **28**, 7510–7516 (1989).
24. Kay, L. E., & Bax, A. *J. Magn. Res.* **86**, 110–126 (1990).
25. Delaglio, F. et al. *J. Biomol. NMR* **6**, 277–293 (1995).
26. Garrett, D.S., Powers, R., Gronenborn, A.M., & Clore, G.M. *J. Magn. Res.* **95**, 214–220 (1991).
27. Nilges, M., Gronenborn, A.M., Brüger, A.T., & Clore, G.M. *Prot. Engng.* **2**, 27–38 (1988).
28. Brünger, A. T. *X-PLOR Version 3.1. A system for X-ray crystallography and NMR* (Yale University Press, New Haven, Connecticut; 1992).
29. Kraulis, P.J. *J. Appl. Crystallogr.* **24**, 946–950 (1991).
30. Nicholls, A. *GRASP: graphical representation and analysis of surface properties* (Columbia University, New York; 1992).
31. Laskwoski, R.A., MacArthur, M.W., Moss, D.S. & Thornton, J.M. *J. Appl. Crystallogr.* **26**, 283–291 (1993).

1998 Nature America Inc. • http://structbio.nature.com